Emergence of negative trophic level-size relationships from a size-based, individual-based multispecies fish model

Morgane Travers-Trolet, Franck Coppin, Pierre Cresson, Philippe Cugier, Ricardo Oliveros-Ramos, Philippe Verley

Emergence of negative trophic level-size relationships from a size-based, individual-based multispecies fish model

Morgane Travers-Trolet [a,b]*, Franck Coppin [a], Pierre Cresson [a], Philippe Cugier [c], Ricardo Oliveros-Ramos [b], Philippe Verley [d]

[a] Ifremer, Channel & North Sea Fisheries Research Unit, RH, 150 Quai Gambetta, 62200 Boulogne-sur-Mer, France.

*corresponding author : Morgane.Travers@ifremer.fr Tel : +33(0)2 40 37 40 99. Fax : +33(0)2 40 37 40 75

[b] Ifremer, Centre Atlantique, EMH, rue de l'île d'Yeu, 44300 Nantes, France

[c] Ifremer, Ctr Bretagne, DYNECO-LEBCO, CS10070, F-29280 Plouzané, France.

[d] AMAP, IRD, CNRS, CIRAD, INRA, Univ Montpellier, Montpellier, France

Abstract

Modeling the mechanisms underlying trophic interactions between individuals allows the food web structure to emerge from local interactions, which constitutes a prerequisite for assessing how marine ecosystems respond to various anthropogenic pressures. Using a multispecies spatially explicit individual-based model, the emergence of trophic patterns was explored in the eastern English Channel ecosystem, where pelagic-benthic trophic coupling was recently studied empirically. The OSMOSE model was applied to this ecosystem by explicitly representing the life cycle of 13 fish species and one squid group, forced by pelagic and benthic prey fields that are variable over time and space. A matrix defining

possible accessibilities between life stages was added to the model to link benthic and pelagic communities through overlap of vertical distribution. After optimizing some parameters of the model to represent the average state of the fish community during the 2000-2009 period, the simulated trophic structure was explored and compared to empirical data. The simulated and stable-isotope-derived trophic levels of fish were in relatively good agreement. Intraspecific variability of the trophic level is high in the five stable-isotope datasets but is well encompassed by the model. Despite the hypothesis of opportunistic size-based predation, the simulation showed a decreasing trend of trophic level with size for four benthic species, a pattern observed empirically for a different set of species in the ecosystem. Model exploration showed that this emerging pattern varies spatially and is both explained by the spatial variability of prey availability and by the independence of trophic and size structures of benthic invertebrates. The combination of individual-based models of stomach contents and intrinsic tracers, such as stable isotopes, appears to be a promising tool to better understand the causes of observed trophic patterns.

Highlights *(3 to 5 bullet points with maximum 85 characters, including spaces, per bullet point)*

- An individual-based model successfully simulates the eastern English Channel food web
- Trophic spectrum of 14 species generally match 2000-2009 stable isotope data
- Intraspecies trophic variability is high, both in the model and the stable isotope data
- The emerging relationship of trophic level with size is negative for four species

Keywords

Emergent patterns; pelagic-benthic coupling; individual-based model; food web; fish community

1. Introduction

Trophic ecology has been investigated empirically for decades in marine ecosystems to better understand key properties of ecosystems, including energy flows in ecosystems, the resilience and adaptation of ecosystems to large-scale pressures and the relationship between biodiversity and ecosystem functioning (Belgrano et al., 2005). The current need to establish an integrated management framework fosters the development of a multitrophic approach, where all interspecific interactions are addressed (Seibold et al. 2018). Initially addressed through stomach content analysis, trophic ecology is now based on various tools, including intrinsic tracers, such as stable isotope ratios and fatty acids (Ramos and González-Solís, 2012). Combining “old” and “modern” techniques is now viewed as the most powerful approach (Cresson et al., 2014) providing both a detailed vision of prey actually consumed and a general picture of trophic fluxes and food web topology. In parallel with these field studies based on biological sampling and chemical analysis, theoretical work has focused either on predator-prey interactions (e.g., Lotka-Volterra) or on network complexity and stability (Belgrano et al., 2005). The development of holistic models allowed the coupling of theoretical and empirical approaches by conceptualizing the food web structure of a particular ecosystem based on data and simulating its dynamics. Typically, Ecopath models (Christensen and Pauly, 1992) aim at balancing the food web structure of an ecosystem of interest based on observed diets and produce network indicators such as the recycling index, average path length and total system throughput (Heymans et al., 2014) but also information about species trophic positions and functions and their impacts on other functional groups.

Partly to increase their realism and partly to answer a wider range of scientific questions, the complexity of ecosystem models has been increasing by integrating temporal (e.g., Ecopath with Ecosim) and spatial

heterogeneity (e.g., Ecospace (Pauly et al., 2000), Atlantis (Fulton et al., 2011)) and by considering age or size structure within a trophic node defined to represent a species or functional group. Such models are currently mostly used to explore ecosystem responses to anthropogenic or environmental pressure, and their potential for theoretical trophic ecology is most likely underused. Trophic information from field studies is required to parameterize links between compartments, at least to identify them and sometimes to set their intensity (i.e., percentage of a prey in the diet of the predator) (Pethybridge et al., 2018). However, this information is at best used at the species level and is often averaged over several species to inform functional group trophic habits. Trophic variability exists among individuals and can be linked to ontogenetic changes, individual variability and composition of the local trophic environment (spatiotemporal heterogeneity) (e.g., Stehlik and Meise, 2000). Instead of reducing this variability to parameterize ecosystem models, in this study, we aim to use a complex modeling approach to explore the individual trophic variability of marine fish. To do so, we used the multispecies individual-based model OSMOSE (Shin and Cury, 2004, 2001; Travers et al., 2009), where fish individuals constitute the structural unit of the model. Individual-based models (IBMs) allow for representing individuals that adapt to their local environment (leading to variability among individuals) and that interact mechanistically with each other and with their environment (both abiotic and biotic, i.e., composed of other individuals). Interactions between these adaptive individuals lead to the emergence of population-level properties (e.g., resilience, spatiotemporal variations of abundance), which are more than the sum of individual properties (Grimm and Railsback, 2013). Applied to trophic ecology, this means that the trophic structure of an ecosystem emerges from local predation interactions between fish individuals (being both prey and predator).

We applied the OSMOSE modeling framework to the eastern English Channel (EEC), where several empirical trophic studies have been recently conducted. The English Channel is an epicontinental sea located between the United Kingdom and France and is subject to environmental forcing (mega tidal

regime and strong influence of rivers) and various human pressures, such as fisheries, aggregate extraction, maritime traffic, and wind farms (Carpentier et al., 2009). The structure and spatiotemporal variation of the fish community has been studied (Vaz et al., 2007), and the trophic links structuring this ecosystem have been recently investigated as well. Cachera (2013) studied the trophic organization of the fish communities through digestive tract contents and geomorphometric measurements to link it to morphological and functional trait variation across and within species. Kopp et al. (2015) investigated the strength of the pelagic-benthic coupling along an inshore-offshore gradient via stable isotope ratios. Giraldo et al. (2017) coupled both approaches to make conclusions regarding the resource use of fish along the depth gradient. These studies showed that bentho-pelagic coupling is strong in the EEC, with benthic sources being important for both benthic and pelagic fish and with a decreasing intensity of the bentho-pelagic coupling as depth increases. In addition to these empirical studies, a holistic model has been applied to the EEC to explore the effects of fisheries management options on the flatfish and demersal fish species (Girardin, 2015). The calibration process of this Atlantis model allowed us to gain better insight into ecosystem functioning and to identify the main drivers of the system, including the importance of nutrient input through rivers and the competition interactions between demersal species (Girardin et al., 2018). While the EEC trophic structure has been investigated through several methods, some of its variability remains unexplained and is assumed to be related to intraspecies and seasonal variations. To address the finer dynamics of the predation process and how it can shape observed patterns at different levels of organization, OSMOSE was applied to the EEC ecosystem to explore the trophic variability of fish individuals.

2. Materials and methods

The individual-based OSMOSE (Object-oriented Simulator of Marine eCOsystems Exploitation, Shin and Cury, 2004, 2001; Travers et al., 2009, www.osmose-model.org) is a spatial model representing the whole life cycle of several fish species from eggs and larvae up to juveniles and adults. This multispecies model is size-structured and based on opportunistic predation that depends only on spatiotemporal cooccurrence and body size ratios between a predator and its prey. Because of this opportunism, neither the a priori food web structure nor the diet matrix are set, but they emerge from local trophic interactions. This model has been applied to a variety of ecosystems, such as upwellings (e.g., Marzloff et al., 2009; Travers-Trolet et al., 2014; Oliveros-Ramos et al., 2017), estuaries (e.g., Brochier et al., 2013), semi-enclosed seas (Fu et al., 2012) and shelf seas (e.g., Grüss et al., 2015; Halouani et al., 2016). The main structure and equations of the model are presented below, before focusing on its application to the EEC. An extended description of the OSMOSE model following the ODD protocol (Overview, Design concepts, and Details) proposed by Grimm et al. (2010) and a description of the R packages dedicated to the model calibration are also available at https://documentation.osmose-model.org/osmose.html.

2.1. Model structure and processes represented in OSMOSE

The individual element of the OSMOSE model is a super-individual of identical fish (Scheffer et al. 1995), i.e., of the same size, same trophic level (TL), same location and belonging to the same species. During each two week time step, the abundance (also called worth) and biomass of each super-individual changes according to the different modeled processes, described below (Figure 1). Only the main features and equations are recalled in this paragraph, and more complete details can be found in Shin and Cury (2004, 2001), Travers et al. (2009), and Travers-Trolet et al. (2014).

At the beginning of the time step, super-individuals are distributed over a 2-dimensional grid. The spatial distribution of fish is driven at the larger scale by presence/absence maps provided as input for each

136 species and possibly for different ages and/or seasons according to available knowledge. When the input
137 distribution map remains the same between two consecutive time steps, super-individuals can move to
138 adjacent cells following a random walk pattern (foraging), while always remaining within the limits of
139 their presence map.

140 After movement, all processes involving local interactions occur: explicit predation on other super-
141 individuals and on plankton and/or benthic invertebrate groups, mortality from this explicit predation,
142 starvation mortality, fishing mortality and mortality from other sources such as top predators. In the real
143 world, such processes are concurrent and concomitant. To approximate real continuous time, the
144 mortality algorithm introduces (i) a subdivision of the time step (here set to 10), (ii) random shuffling of
145 super-individuals and mortality processes within every time step and (iii) asynchronous updating of the
146 state variables (i.e., super-individual biomass is updated as the model goes through the processes)
147 (Caron-Lormier et al., 2008). The predation process first assesses the food requirement for each super-
148 individual, based on the maximum ingestion rate *r* of the predator *i*. This value is then compared to the
149 amount of suitable food available locally, i.e., in the cell of the predator, defined by the suitability of prey
150 size compared to predator size, the biomass B_j of each prey available and an accessibility coefficient $a_{i,j}$
151 representing vertical overlap and/or morphological constraints between the prey *j* and the predator *i*.
152 Depending on the available biomass of prey, a predator can thus eat an amount of food varying between
153 0 (no prey of suitable size available) and its maximum ingestion rate. The predated biomass $PB_{i,j}$ of a prey
154 *j* by a predator *i* is expressed as follows:

155 $$PB_{i,j} = min\left(rB_i \frac{a_{i,j}\,B_j}{\sum_k a_{i,k}\,B_k}\ ,\ a_{i,j}\,B_j\right) \qquad \text{(Equation 1)}$$

156 The predation pressure is applied to all prey, proportional to their relative contribution to the total
157 amount of edible food (i.e., no preference). Predation mortality is then applied to the preyed super-
158 individual by reducing its abundance and biomass according to the realized predation pressure, possibly

leading the super-individual to disappear if abundance falls below 1. According to the amount of food eaten compared to its maximum ingestion, the predation efficiency ξ is computed for each super-individual *i*. If ξ_i falls below the threshold corresponding to maintenance requirement ξ_{crit}, the starvation mortality rate M_ξ is positive and increases linearly with predation efficiency reduction (Equation 2).

$$M_\xi = \frac{-M_{\xi\max}}{\xi_{\text{crit}}}\xi_i + M_{\xi\max} \qquad \text{(Equation 2)}$$

The different mortality rates (starvation M_ξ, fishing F and other sources M_{oth}) are applied similarly to decrease the abundance of a super-individual *i* following the survival formula (Equation 3).

$$N_{i,t+\Delta t} = N_{i,t}e^{-\Delta t M_x} \quad \textit{with } M_x \in \{M_\xi, F, M_{\text{oth}}\} \qquad \text{(Equation 3)}$$

The fishing mortality rate is species-specific, but can vary temporally and/or spatially according to available knowledge. For the fishing process, knife-edge selectivity was used, affecting only recruited fish i.e., fish older than the species age at recruitment. Finally, mortality from other sources is also considered by taking into account predation by organisms nonexplicitly represented in the model (e.g., other fish, birds, mammals) as well as diseases and senescence. A particularly high mortality term is applied to the first stages (eggs) to represent the bottleneck of survival due to nonfertilization of eggs, starvation of first-feeding larvae, advection, sinking and predation by nonexplicitly modeled organisms. Because very little quantification exists on these processes, the larval mortality rates are calibrated (see section 2.4).

After this loop of interaction processes, growth can occur if the predation was successful enough, i.e., if the biomass eaten is higher than maintenance requirements. The length increment depends on the predation efficiency and averaged length increment (ΔL) at the super-individual's age derived from the

von Bertalanffy growth curve (Equation 4). The weight *W* of an individual increases simultaneously with its length through an allometric relationship.

$$\begin{cases} \Delta L_{i,t} = 0 & \text{if} \xi_i < \xi_{\text{crit}} \\ \Delta L_{i,t} = \frac{2\Delta L}{1-\xi_{\text{crit}}}(\xi_i - \xi_{\text{crit}}) & \text{if} \xi_i > \xi_{\text{crit}} \end{cases} \quad \text{(Equation 4)}$$

Finally, the time step ends with the reproduction process, where new super-individuals of eggs are produced, depending on the spawning stock biomass (computed from a sex ratio of 1:1 and from the biomass *B* of all fish older than age at maturity A_{mat}), the species relative fecundity φ and the seasonality of spawning s_t (Equation 5).

$$N_{0,t} = \varphi s_t \frac{1}{2} \sum_{a>A_{mat}} B_{a,t} \quad \text{(Equation 5)}$$

2.2 Application to the eastern English Channel

The EEC ecosystem is modeled with OSMOSE through the explicit consideration of 14 species, which constitute 80% of the international landings from this area (ICES area 7d, excluding invertebrates) and more than two-thirds of the fish biomass sampled during the scientific bottom trawl Channel Ground Fish Survey (CGFS, Coppin and Travers-Trolet 1989). This set of species is composed of mackerel (*Scomber scombrus*), horse mackerel (*Trachurus trachurus*), sardine (*Sardina pilchardus*), herring (*Clupea harengus*), poor cod (*Trisopterus minutus*), cod (*Gadus morhua*), whiting (*Merlangius merlangus*), pouting (*Trisopterus luscus*), red mullet (*Mullus surmuletus*), dragonet (mostly *Callionymus lyra*), lesser spotted dogfish (*Scyliorhinus canicula*), sole (*Solea solea*), plaice (*Pleuronectes platessa*) and squids (*Loligo forbesi* and *Loligo vulgaris*). Species parameters are reported in Table 1 and are mostly derived from Carpentier et al. (2009) but also from other literature or online databases (Appendix A). The modeled area extends from 49°N - 2°W to 51.2°N - 2.5°E and is composed of 445 cells of 0.6° x 0.6°

(Figure 2). Presence/absence maps per species, and per season and/or age class when available, have been computed from survey data and available literature (Appendix B). Two species migrate out of the English Channel towards the North Sea: adult horse mackerel from July to September and herring from April to September. When these species are out of the modeled area, they grow following the von Bertalanffy curve (Table 1) and undergo an additional mortality of 1.05 $year^{-1}$ and 0.55 $year^{-1}$, respectively (values derived from an Ecopath model applied to North Sea, Mackinson and Daskalov, 2007). Reproductive seasonality of each species is reported in Appendix C, while the fishing mortality rate is considered constant over the seasons for all species except for squids (fishing closure from May to mid-July) and horse mackerel (increased fishing mortality rate from October to December).

2.3 Forcing prey fields: planktonic and benthic groups

During the predation process, super-individuals can feed both on other explicitly modeled fish and on low trophic level (LTL) sources. LTL groups are integrated in OSMOSE through the forcing of biomass prey fields. Plankton prey fields come from the ECO-MARS3D biogeochemical model applied to the English Channel (Le Goff et al., 2017; Vanhoutte-Brunier et al., 2008) with a grid of 2 km horizontal resolution and 10 vertical layers. The nutrients and plankton dynamics simulated with this model have been validated with data from monitoring stations and correctly reproduce the interannual variability observed in the English Channel (Le Goff et al., 2017). The biomasses of two phytoplankton groups (grossly representing dinoflagellates and diatoms) as well as microzooplankton and mesozooplankton groups have been integrated vertically and over the 2-week time step of OSMOSE to be used as forcing prey fields. Furthermore, as the current application aims at simulating the EEC ecosystem at a stable state, plankton climatology was created by averaging data bimonthly from the 2000-2006 period (Appendix D). Six additional LTL groups were added to complement the LTL food source available to fish:

224 a macrozooplankton group (representing both holoplankton and meroplankton mostly composed of
225 benthic invertebrate larvae) and five benthic groups of different sizes (Table 2). As available information
226 on the spatial distribution of these groups was not sufficient, they were considered to be
227 homogeneously distributed.

228 The grid used in OSMOSE has no vertical dimension; therefore, accessibility coefficients were used to
229 represent vertical overlap both among super-individuals and between super-individuals and LTL groups
230 in the computation of prey biomass available for predators. According to their ecology, each stage of
231 each species and each LTL group was associated with a vertical layer: “pelagic” for plankton, buoyant
232 eggs, larvae and small pelagic fish, “benthic” for benthic groups and species living on the seabed such as
233 flatfish, and “demersal” for individuals living near the sea bed and having access to both pelagic and
234 benthic prey (such as gadoids). The accessibility parameters are presented in Table 3.

235

236 ### 2.4 Calibration

237 The model was calibrated using the calibrar R package with the AHR-ES algorithm (Oliveros-Ramos and
238 Shin, 2016), an automatic evolutionary algorithm developed for calibrating stochastic models such as
239 OSMOSE. This algorithm explores a range of values for unknown parameters and uses likelihood
240 objective functions to select the optimal values for the catches and biomass to be comprised within
241 ranges of observed values when available. Landings per species have been extracted from the ICES
242 Fisheries Statistics official database (ICES, 2011a) for the ICES area 7d (corresponding to the EEC) over
243 the period 2000-2009. Total stock biomass estimates are directly available from stock assessment
244 reports for sole and plaice (ICES, 2011b), while for whiting, cod, mackerel and herring, total stock
245 biomass estimates were derived from stock assessments covering a wider area (ICES, 2012, 2011b) and
246 were therefore scaled to the EEC proportional to the relative landings in this area. In OSMOSE, species

biomass is computed as the sum over the entire area of the biomass of all super-individuals older than 6 months, averaged annually. Simulated landings come from the fished individuals (equation 3) over the entire area, integrated at the annual time-scale. The calibration was performed in 3 phases, following recommendations by Oliveros-Ramos et al. (2017) based on model dependency of the parameters and availability of initial estimates. First, the 10 LTL accessibility coefficients were adjusted for 200 generations; then, the 14 larval mortality rates were added to the set of parameters to adjust for 200 other generations. Finally, 12 additional mortalities (including fishing mortalities) were added to the third phase, where 300 generations were run with a total of 36 parameters to estimate. The first two phases allow optimization of the calibration convergence, while the third phase includes all the parameters and lasts longer to ensure that an optimal solution is reached.

2.5 Scenarios and exploration of simulated trophic patterns

Once the model is calibrated, it is run for 120 years, with the first 100 years corresponding to the spin-up time during which the system stabilizes and is no longer driven by the model initialization. The results presented thereafter, corresponding to the average state of the EEC ecosystem in the period 2000-2009, are computed from averaging the last 20 simulated years to smooth any interannual variability. Furthermore, OSMOSE is a stochastic model, and 50 replicates were run using the same input parameters.

Following the pattern-oriented modeling approach (POM, Grimm et al., 2005), the model's ability to reproduce independent patterns is explored by comparing simulated output with data neither used during the parameterization nor during the calibration. As the OSMOSE model is based on opportunistic predation, validation patterns could include emerging features linked to the predation process, such as realized diets and associated TLs or food web structures. Here, we used independent data of TLs

calculated from nitrogen stable isotope ratios (SI) measured on the same species in the same ecosystem (Cresson et al., 2017, 2018; Jennings and van der Molen, 2015; Kopp et al., 2015, Mialet et al., 2017). TL calculations are based on the premise that the nitrogen isotopic ratio ($\delta^{15}N$ hereafter) is gradually enriched at each TL, a phenomenon called trophic enrichment. TL is thus considered as the isotopic difference between the species of interest and a trophic baseline, i.e., a proxy of the ultimate organic matter source at the base of the food web, divided by the trophic enrichment factor (TEF). The queen scallop *Aequipecten opercularis* was used as a trophic baseline due to the trophic importance of benthic production and because the use of a primary consumer (i.e., at TL = 2) allows smoothing of the small scale isotopic fluctuations of primary production that are not integrated in fish isotopic ratios. Two methods are used, where TEF is either considered the same at all levels of the food web (e.g., in Kopp et al., 2015; Cresson 2017; 2018; Mialet et al., 2017) or decreases with increasing $\delta^{15}N$ of the diet (Jennings and van der Molen, 2015). Details about the method can be found in dedicated literature (Hussey et al., 2014), but sensitivity analyses demonstrated that for intermediate-TL species such as the ones considered in the present study, calculated TLs are rather similar regardless of the method (Jennings and van der Molen, 2015; P. Cresson unpubl. results).

In OSMOSE, each super-individual has a proper TL, which depends on its feeding history. The TL computation of a super-individual *i* is based on the classical formula in which the TL of a predator equals 1 plus the average TL of the prey weighted by their relative ingested biomass (Equation 6):

$$TL_{i,t} = 1 + \sum_j TL_{j,t} DC_{j,i,t} \qquad \text{(Equation 6)}$$

where $TL_{i,t}$ is the trophic level of *i* at time *t* and $DC_{j,i,t}$ is the proportion of prey *j* in the diet of predator *i* at time *t*. While the TL of explicitly modeled individuals is dynamic, the TL of the LTL groups is fixed and has been set to 1 for phytoplankton and derived from TL estimates based on stable isotope studies in the same area (Kopp et al., 2015) for the other groups (Table 2). The TL of very small benthos is set to 3 to

represent the omnivory of this group (partly composed of meiofauna). The TL of newly spawned eggs within OSMOSE is arbitrarily set to 3 to be close to the TL of the first-feeding larvae. Finally, we assume that an individual that has not fed keeps its previous TL.

After comparison of simulated TLs with data, model exploration is performed by analyzing the variation of diet composition and TL with size for all species. Diet composition is computed using the following predefined size classes for predators: [0;5[, [5;10[, [10;15[, [15;20[, [20;25[, [25;30[, [30;40[, [40;50[, [50;60[, [60;70[, [70;90[, [90;110[and [110;130[. From all super-individuals pertaining to a size-class, the biomasses of the different prey eaten (including other super-individuals and LTL groups) are grouped by species over the entire area. To explore the relationship between TL and size, super-individuals are grouped by centimeters and the TL distribution within each size group is computed (min, first quartile, median, third quartile, max). The TL-size relationship is then explored spatially by fitting a linear model in each cell with more than 10 super-individuals. The resulting slope values are then mapped for each species, with indication of the quality of the fit using R^2 values.

3. Results

The evolutionary algorithm used for calibrating the model converged to an acceptable configuration where all median values of simulated biomass distribution are within the range of observed values (Figure 3). Median values of simulated catches are within the range of observations for half of the species (lesser spotted dogfish, whiting, cod, mackerel, sardine and squids), while for red mullet, horse mackerel and herring, catches are underestimated as only 42%, 42% and 18% of the 50 simulated replicates are within the range of the observations, respectively. Simulated catches of pouting, sole and plaice are smaller than the observations (median values corresponding to 73%, 57% and 80% of the minimal observed values, respectively), even if the biomass of the flatfish species corresponds to the

316 total stock biomass estimates through the stock assessment (ICES 2011). For the other assessed species
317 (whiting, cod, mackerel and herring), simulated biomass also displays a good fit to biomass estimated
318 over the period of 2000-2009. The optimized values of accessibility parameters show high variability
319 across the LTL groups, from approximately 10^{-4} for dinoflagellates to approximately 0.4 for meso-
320 zooplankton and very large benthos (Table 2), two important prey groups for the fish community.

321 A comparison of simulation outputs with published TLs from empirical SI analysis is performed as a
322 validation process. Figure 4 displays the trophic spectra of the modelled species, i.e., for each species,
323 the distribution of the individual TL weighted by the individual biomass. In the simulations, the width of
324 the trophic spectrum (i.e., the difference between the maximal and minimal individual TLs) varies
325 according to species from 1.6 levels for red mullet up to 3.9 levels for herring. More importantly, the way
326 biomass is distributed along TLs also varies: for some species, biomass distribution is concentrated
327 around a particular TL (e.g., approximately 3.9 for red mullet, pouting, poor cod, dragonet, sole), while
328 for other species, biomass is spread over a wide range of TLs (e.g., whiting, cod, sardine, squids). The
329 biomass concentration of approximately 3.9 for benthic fish species is linked to the dominant proportion
330 of very small benthos and small benthos (TL=3 and TL=2.9, respectively, Table 2) in the diet of these
331 species (Figure 5). Plaice individuals of intermediate length (15-50 cm) also largely rely on these prey
332 groups, explaining the concentration of biomass around TL=3.8 in the trophic spectrum (Figure 4). The
333 biomass around TL=4.5 is explained by the presence of very large benthos (TL=3.6) in the diet of larger
334 plaice individuals. The wide trophic spectra of lesser spotted dogfish, whiting and cod are explained by
335 the diversity of prey composing their diets (Figure 5).

336 Simulated trophic spectra were in good agreement with the range of TLs estimated from stable isotope
337 measurements for most species. For red mullet, poor cod, and plaice, simulated TLs were similar to SI-
338 derived TLs, which were, moreover, coherent between empirical studies. For lesser spotted dogfish,

pouting, whiting, sole, horse mackerel and mackerel, empirical data display high variability across studies, but this variability is generally well encompassed by the model. However, empirical TL estimates show that the maximal TL observed for sole can be higher than that simulated, while mackerel can have a minimal SI-derived TL smaller than that simulated. It is worth noting that for mackerel, the model simulates two TL modes, approximately 3.6 and 4.3, corresponding respectively to young individuals feeding only on mesozooplankton (TL=2.6, Table 2) and larger individuals feeding on small squids and small fish, mostly young sardine and horse mackerel (Figure 5). Similarly, empirical estimates of mackerel TL show low values of approximately 3.5 in Cresson et al. (2017) and Jennings and van der Molen (2015), with fish being between 16.9 and 41 cm long (Table 4), while TL values are higher than 4 in the three other studies but for similar fish lengths (18 to 34 cm, Table 4). If we assume that TL estimated from stable isotopes are representative of the trophic position of the bulk of a species, then the EEC-OSMOSE model tends to slightly overestimate the TL of cod, dragonet and squids and to underestimate the TL for herring. The SI-derived TL of sardine corresponds to the bulk of the simulated biomass, but the model also simulates sardine individuals at a TL between 2 and 3 (feeding on diatoms and mesozooplankton, Figure 5).

To further explore the drivers of individual variability among species TL distribution, the evolution of the mean TL with size is presented in Figure 6. While mean TL generally increases with size for most species, this is not the case for red mullet, poor cod, dragonet, and sole and for pouting and plaice to a lesser extent (respectively, from 10 to 35 cm and from 20 to 50 cm), for which the mean TL decreases with size. These species are characterized by a benthic diet, with the proportion of very small benthos (TL=3) decreasing with size and the proportion of medium benthos (TL=2.2) increasing as fish grow larger, which explains the decreasing TL with size for these species. The evolution of mean TL with size is not linear, and most species display a strong change of TL at smaller size, while mean TL varies less with size for larger individuals. Tipping points can be identified and linked to ontogenetic changes in the diets of

363 species. For instance, sardine and herring fish longer than 20 cm no longer feed on diatoms (Figure 5),
364 explaining the abrupt TL increase at this size. Other ecological features can be observed, such as the
365 marked shift from a plankton-feeding larval stage (roughly for fish smaller than 5 to 10 cm on Figure 6) to
366 a benthic feeding juvenile stage for all benthic and demersal species. Finally, other TL breakpoints linked
367 to diet shifts exist for larger fish: the occurrence of very large benthos for lesser spotted dogfish larger
368 than 30 cm, pouting larger than 35 cm, whiting larger than 15 cm, cod larger than 20 cm and plaice larger
369 than 50 cm, and the disappearance of mesozooplankton for horse mackerel and mackerel larger than 20
370 cm. To supplement the patterns observed over the entire area between TL and size, the spatial
371 distribution of the TL-size relationship is mapped (Figure 7). The negative relationship between TL and
372 size is confirmed in every grid cell for red mullet, dragonet and sole. This pattern appears robust (R^2 >
373 0.3) in the Dover Strait (Northeast), in the north of the Central English Channel (Northwest) and in the
374 Bay of Seine (South). For poor cod, another species showing a decreasing TL-size relationship at the
375 global scale, the spatial distribution of the slope is less informative (R^2<0.3) but shows both positive and
376 negative relationships (the latter occurring also in the Dover Strait and north of the Central English
377 Channel). For plaice and pouting, the relationship is positive in most cell grids and is probably driven by
378 the strong difference of TL between fish of intermediate size and larger fish. Robust positive
379 relationships between TL and size also occur for pouting, herring, sardine and squids.

380

381 **4. Discussion**

382

383 4.1 Ability of the model to capture EEC ecosystem dynamics

384

In this study, we were able to adapt the 2D OSMOSE model using a vertical overlap matrix and apply it to the EEC shallow ecosystem characterized by strong bentho-pelagic coupling. After parameterizing the model, the semiautomatic calibration method produced an overall good fit of the model to the 2000-2009 average state of the EEC ecosystem, with biomass of all species and catch values of half of the species being within the range of the observed values. The discrepancies observed for some species between modeled and observed catches and biomasses can be explained by several factors. First, a constant fishing mortality is applied in OSMOSE to individuals older than the age at recruitment (i.e., similar to broken-stick selectivity with age), while in reality due to the different fleet selectivity and variable catchability-at-age, the fishing pressure endured by fish varies with age/length (Quinn and Deriso, 1999). Nonetheless, it is worth noting that the total mortality varies with age within OSMOSE, notably due to explicit predation mortality, which tends to decrease with size. Second, the biomass target values come from single-stock assessments, i.e., correspond to model outputs with specific hypotheses and thus should be taken as estimates with associated uncertainty rather than exact values (Brooks and Deroba, 2015). Similarly, target catch values come from declared landings completed by estimates of discards when available. Even if the EEC is considered a data-rich ecosystem, some uncertainties persist when estimating discards and total catches (Enever et al., 2007; Pauly and Zeller, 2016). Furthermore, the hypothesis made to allocate the biomass of widely distributed stock to the ICES 7.d area based on the landings ratio does not take into account the spatial variability of fishing effort and assumes a homogeneous distribution of fish, again contributing to the uncertainty around biomass target values. Third, the calibration process was limited to the optimization of 36 unknown parameters, therefore constraining the space of simulated output reachable during the calibration.

Despite these limits, the model was able to reproduce species biomasses and most species catches, but also other features independent of the data used for parameterization and calibration. For most species, the simulated TLs are in good accordance with TL estimates derived from SI data, both in terms of

409 average values and variability within species. However, EEC-OSMOSE underestimates sardine and herring
410 mean TLs compared to SI estimates. The exploration of simulated TL and diet composition versus size
411 shows that the smaller size classes have a diet mostly composed of diatoms and mesozooplankton
412 (resulting in small TL values), while the larger individuals rely on mesozooplankton, explaining their
413 higher TL. One hypothesis for the difference observed between the data and the model is that empirical
414 data underestimate the importance of phytoplankton food source. This could be explained by the
415 absence of very small individuals (smaller than 5 cm for herring, smaller than 7.7 cm for sardine, Table 4)
416 in the sample, and/or by the sampling season (autumn) corresponding to higher zooplankton food
417 available compared to phytoplankton. Another hypothesis is the biased simulation of diet shift from
418 phytoplankton to zooplankton prey at larger size than observed for herring and sardine. Both species are
419 known to consume these two types of prey, with seasonally variable intensity (Costalago et al., 2012),
420 but the ontogenetic shift in their diet has been reported at an earlier larval stage (e.g., Denis et al.,
421 2016). These results suggest that the minimum and maximum predation size ratios set for herring and
422 sardine may be revised, possibly by setting different ratios according to individual ontogenetic
423 development (e.g., Travers-Trolet et al., 2014). Moreover, due to the model structure and lack of suitable
424 stable isotope data, the mesozooplankton group has a fixed TL that prevents simulation of the
425 spatiotemporal variability of the TL of the zooplankton community available to fish. It should
426 nevertheless be remembered that fish stable isotope ratios (and the derived TL values) can be seen as
427 emergent properties, resulting from their diet but also from a large set of environmental or physiological
428 parameters (e.g., Boecklen et al., 2011). Among these, large spatial and temporal variations of
429 phytoplankton isotopic ratios (Magozzi et al., 2017) at the basis of the food web and/or fish migrations
430 between zones where primary production exhibits different isotopic ratios may drive changes in fish
431 isotopic ratios that are hard to capture and that may blur TL calculation.

The overestimation of the trophic position of cod in the model comes with an overestimation of the proportion of fish in the diet. The model simulates the proportion of fish biomass in cod diets as between 50% and 80% according to size classes, while fish represent nearly one quarter or less of the prey found in stomach content analysis (crustaceans being the main prey for juveniles and adults, Cachera, 2013; Pinnegar 2014; Mialet et al., 2017). This bias is due to the relatively simple accessibility matrix set for representing the proportion of prey biomass available to a predator according to their vertical distributions. For this matrix, cod is considered to be demersal, i.e., to have full access to other demersal individuals and to have access to half of the pelagic biomass and half of the benthos biomass. To better represent the feeding behavior of cod, accessibility coefficients should be revised, for instance by increasing accessibility to benthic prey and reducing accessibility to pelagic and demersal individuals. For this study, the accessibility matrix was introduced to mimic vertical overlap between predators and prey as required to model both benthic and pelagic communities with an opportunistic size-based predation, but its parameterization was kept as simple as possible. For their coupled size-spectrum model, Blanchard et al. (2009) considered that all predators spent half of their time feeding on benthic invertebrates and the other half feeding on pelagic organisms. Future developments on how to better set these accessibility parameters could involve consideration of the spatial variability of trophic interactions (e.g., depth-driven variability in bentho-pelagic coupling; Giraldo et al., 2017) or use morphological attributes (trait-based approach) of the different species (e.g., orientation of the mouth).

4.2 Relationship between size and TL

When considering TL with regard to size for the different species modeled, two main patterns emerge from the simulations. The most frequent pattern is an increase of TL as size increases, which is often

455 more pronounced for the smaller size classes. This positive relationship can display some breakpoints
456 linked to diet composition shifts, as illustrated by planktivorous fish species at 20 cm. The second pattern
457 is observed for only four benthic species (red mullet, poor cod, dragonet and sole) and corresponds to a
458 decrease of TL with increasing size. For the small individuals of these four benthic species (smaller than
459 5-10 cm), the initial increase in TL is explained by the pelagic and planktivorous mode of the larvae
460 before settlement on the sea bottom, modeled through change of the accessibility predation coefficient
461 (Table 3).

462 In aquatic ecology, the assumption that larger individuals have a higher TL is often admitted, as
463 predation is constrained by body size through gape limitation. Such a relationship has been explored and
464 confirmed across species in various ecosystems by confronting the mean or maximum size of species
465 with their mean $\delta^{15}N$ (e.g., France et al., 1998; Romanuk et al., 2011). However, other studies have
466 reported an absence of correlation between species mean length and their trophic position (e.g., Layman
467 et al., 2005). Jennings et al. (2001) also documented a weak cross-species relationship between the
468 maximum size of fish species and their mean $\delta^{15}N$ value but a strong relationship at the community level,
469 i.e., using the individual length of fish and pooling the data together within size classes. The ontogenetic
470 increase of TL with increasing size has also been confirmed for benthic fish species by Badalamenti et al.
471 (2002). Investigating the North Sea trophic structure, Jennings et al. (2002a) found a significant positive
472 relationship between fish length and $\delta^{15}N$ for 16 species over 31. More interestingly, this relationship
473 was found to be negative for herring and plaice whose TL decreases as their length increases. In addition,
474 the pattern observed may be positive in one environment but negative in another (Jennings and van der
475 Molen 2015). The results obtained in the present study thus demonstrate that the variability may appear
476 at even a lower spatial scale, confirming the call for a better understanding of the effect of
477 environmental gradients on trophic functioning (Ings et al., 2009). Based on stable isotope data in the
478 EEC, Kopp et al. (2011) confirmed this decreasing trend of TL with size for plaice but also for skates and

479 even for whiting in some particular habitats (located in the central Bay of Seine and part of the Dover
480 Strait). In half of the region × species combinations they studied, Jennings and van der Molen (2015)
481 observed no relationship between mass and TL, and the positive relationships mostly occurred for
482 piscivore species. As they have to capture mobile prey, gape size is a key factor driving feeding abilities in
483 these species. In benthic systems, feeding mechanisms could be more based on opportunistic predation
484 of carrion and living organisms. In this context, prey size may not be as important in driving the feeding
485 mechanism as for pelagic systems.

486 While based on opportunistic size-based predation, OSMOSE was unexpectedly able to reproduce
487 decreasing trends of TL with size for some benthic species. In EEC-OSMOSE, the benthic species
488 demonstrating a clear declining TL trend with size are not the same as the benthic species found to
489 display this pattern empirically. However, it is worth noting that the empirical negative relationship
490 found for plaice between 9 and 48 cm (Jennings et al. 2002a) is partly present in the model if we focus on
491 intermediate-sized individuals, i.e., before the introduction of very large benthos in the diet (at about 50
492 cm).

493 Being able to reproduce the negative TL-size relationship using such a model allows for drawing two
494 nonexclusive hypotheses of its origin. First, the spatial distribution of fish individuals changes with age
495 (Appendix B), which may result in different prey compositions being available locally, including the case
496 where only prey with lower TLs are available in the area inhabited by larger fish individuals. The spatial
497 distribution of the TL-size relationship confirms this spatial heterogeneity for some species. Thus, the
498 absence of squid eggs in the Dover Strait and the North Central Channel is linked to the strong TL-size
499 negative relationship observed in these areas, where the benthic fish diet is only composed of benthic
500 invertebrates. For mackerel, the absence of juveniles in the Bay of Seine explains the spatial
501 heterogeneity of the signal and suggests that a negative TL-size relationship could be observed

empirically if focus was placed on the adults of this region. In the current model, spatially homogeneous benthic prey fields were used because insufficient knowledge of benthos dynamics was available at this scale. The simulated trophic spatial variability would probably be higher if a more realistic benthic community was included in the model.

The second hypothesis underlying the simulated pattern is that, conversely to what is largely admitted for the pelagic prey, the trophic structure of the benthic prey is not linked to the size structure of the benthic invertebrate community. In the diet of the simulated benthic fish, the increasing proportion of medium benthos with a small TL compared to the proportion of small benthos with a higher TL leads mathematically to a TL decreasing with size at the predator level. This pattern is linked to the predation hypothesis underlying the model and reflects the actual opportunistic pattern of the benthic fish species that consume the most available resources (van Denderen et al., 2018). The selection of species used to set the TL of the benthic groups could have an impact on the overall TL-size relationships of fish. However, they were selected because of their abundance in the area, therefore they were considered suitable to represent the main prey available for fish. Only a few studies have investigated the relationship between size and trophic position for marine benthic invertebrates. Jennings et al. (2002b) demonstrated that for benthic invertebrates, the relationship between size and TL reflected intraspecific patterns (i.e., individual growth) and not interspecific patterns (i.e., no evidence for a relationship between maximum body size and TL across species). Similarly, Dinmore and Jennings (2004) observed a negative relationship between TL and body mass, demonstrating that body dimension may not be a major driver of predation in benthic systems. In their coupled size-based model, Blanchard et al. (2009) confirmed that benthic invertebrates share a common size-unstructured resource and therefore are not strongly trophically size-structured. In other words, two benthic invertebrates of different sizes can exhibit the same TL as their diet would be the same. An ontogenetic diet change in the predator could thus result in an inconclusive or decreasing length-TL pattern.

4.3 Variability of TL across sources

The current study benefited from the existence of several stable-isotope analyses performed in the EEC. Here, we used the available TL estimates at the individual level and explored the intraspecies variability of SI-derived TLs, which increased both with the number of fish individuals sampled and with the width of body sizes sampled (Table 4). The high variability of TLs within a species was confirmed by the model, where individuals can have different TLs depending on their size (involving different size ranges of available prey), their spatial location (local encounters with different prey) and the feeding history of their prey (leading to different TLs of the prey). While the intraspecific TL variability from stable isotopes was required to validate the emergent patterns of the model, the comparison of TL values between different SI studies was also informative. Indeed, the agreement observed between the five studies (e.g., plaice) increases the reliability of these estimates, both in terms of value and width of distribution. For sardine, the very similar TL distribution observed between two studies counterbalances the low number of individuals sampled (10 in each study) and therefore improves the reliability of these data. While the five empirical studies provided similar estimates of species mean TLs and variability for some species, they can lead to different estimates of the TL for other species (e.g., the lesser spotted dogfish mean TL goes from 3.5 to 4.8; the whiting mean TL ranges from 4 to 5.1). Discrepancies between the empirical studies (and with the model) can be due to differences in sampling dates and therefore temporal variation of diet and integration dynamics (seasonal and/or interannual, e.g., Schafer et al., 2002), the spatial location of sampling and its effect on diet (Kopp et al., 2015; Giraldo et al., 2017), the variability of the trophic baseline used (Magozzi et al., 2017) or hypothesis regarding TEF (Hussey et al., 2014). These intraspecific variations are nonetheless classically observed (e.g., Jennings and van der Molen, 2015).

549 Isotopic data allowed validation of the model, but other trophic data sources could have been used to
550 provide a complementary vision. Comparison with stomach content data allowed for a better
551 understanding of the discrepancies regarding the cod TL; the TL overestimation is linked to the
552 overestimation of fish in the cod diet composition. Both isotopic and stomach content data sources are
553 now considered complementary (e.g., Cresson et al., 2014; Giraldo et al., 2017), the latter one informing
554 a snapshot diet with identified prey, while the former integrates trophic fluxes over months and allows
555 us to quantify the fluxes between predators and a pool of prey of similar isotopic signatures. The
556 ecosystem model can now be added to the list of available tools to explore trophic function and
557 individual variability of TLs and could be used in a similar way to explore individual variability across
558 seasons and/or space (i.e., at different depths).

559

560 **5. Conclusion**

561 Using a multispecies IBM constrained by size-based opportunistic predation, we were able to reproduce
562 the average trophic structure of the EEC over 2000-2009, including benthic and pelagic communities.
563 Due to the individual variability in terms of size, spatial location and feeding history, the model
564 simulations displayed patterns that were observed in empirical studies but were unexpected from a size-
565 based predation approach. Here, the IBM framework has been shown to be effective in investigating
566 among-individual trophic variability and for understanding the plausible drivers of the negative TL-size
567 relationship observed empirically for some species. The uncoupling of the trophic structure and size
568 structure of benthic invertebrates appeared to be the key to this pattern, but future studies should
569 further explore this potential link and identify morphological aspects to better represent the predation
570 of fish on benthic invertebrates. The availability of TL estimates from stable isotopes has been a key to
571 validating the model and encouraging strong collaborations between modelers and field/laboratory

scientists. Indeed, while trophic data are often used to parameterize or validate ecosystem models (Pethybridge et al., 2018), complex models - and particularly IBMs - appear useful to inform on the trophic functioning of an ecosystem and to explore different hypotheses regarding the causes of observed patterns. As the trophic patterns simulated with OSMOSE have been validated for the EEC, the model will now be available to explore the ecosystem impacts of different scenarios, including management measures and climate change. The flexibility of the food web structure emerging from local interactions in OSMOSE appears promising when aimed at exploring the cumulative impacts of different pressures.

6. Acknowledgments

This study was partly funded by the European Community's Seventh Framework Programme (FP7/2007e2013) under Grant Agreement No. 266445 for the project VECTORS of Change in Oceans and Seas Marine Life, Impact on Economic Sectors (VECTORS), by the French project EMIBIOS (FRB, contract no. APP-SCEN-2010-II), and by the French government and the region Hauts-de-France under the framework of the project CPER 2014-2020 MARCO. The authors acknowledge the Pôle de Calcul et de Données Marines (PCDM, http://www.ifremer.fr/pcdm) for providing DATARMOR storage and computational resources.

7. References

Badalamenti, F., D'Anna, G., Pinnegar, J., Polunin, N., 2002. Size-related trophodynamic changes in three target fish species recovering from intensive trawling. Mar. Biol. 141, 561–570. doi:10.1007/s00227-002-0844-3

Belgrano, A., Scharler, U.M., Dunne, J., Ulanowicz, R.E., 2005. Aquatic Food Webs: An Ecosystem Approach. OUP Oxford.

Blanchard, J.L., Jennings, S., Law, R., Castle, M.D., McCloghrie, P., Rochet, M.-J., Benoît, E., 2009. How does abundance scale with body size in coupled size-structured food webs? J. Anim. Ecol. 78, 270–280. doi:10.1111/j.1365-2656.2008.01466.x

Boecklen, W.J., Yarnes, C.T., Cook, B.A., James, A.C., 2011. On the use of stable isotopes in trophic ecology. Annual Review of Ecology, Evolution, and Systematics 42, 411–440. doi:10.1146/annurev-ecolsys-102209-144726

Brochier, T., Ecoutin, J.M., Morais, L.T. de, Kaplan, D.M., Lae, R., 2013. A multi-agent ecosystem model for studying changes in a tropical estuarine fish assemblage within a marine protected area. Aquat. Living Resour. 26, 147–158. doi:10.1051/alr/2012028

Brooks, E.N., Deroba, J.J., 2015. When "data" are not data: the pitfalls of post hoc analyses that use stock assessment model output. Can. J. Fish. Aquat. Sci. 72, 634–641. doi:10.1139/cjfas-2014-0231

Cachera, M., 2013. Implications of morphological and functional traits for trophic relationships within fish communities and marine trophic network architecture. Université Sciences et Technologies de Lille. https://archimer.ifremer.fr/doc/00195/30603/

615 Caron-Lormier, G., Humphry, R. W., Bohan, D. A., Hawes, C., & Thorbek, P. (2008). Asynchronous and
616 synchronous updating in individual-based models. Ecological Modelling, 212(3-4), 522-527.
617 doi:10.1016/j.ecolmodel.2007.10.049
618 Carpentier, A., Coppin, F., Curet, L., Dauvin, J.-C., Delavenne, J., Dewarumez, J.-M., Dupuis, L., Foveau, A.,
619 Garcia, C., Gardel, L., Harrop, S., Just, R., Koubbi, P., Lauria, V., Martin, C., Meaden, G., Morin, J.,
620 Ota, Y., Rostiaux, E., Smith, B., Spilmont, N., Vaz, S., Villanueva, C.-M., Verin, Y., Walton, J.,
621 Warembourg, C., 2009. Atlas des Habitats des Ressources Marines de la Manche Orientale -
622 CHARM II, Channel Habitat Atlas for marine Resource Management - CHARM II.
623 https://archimer.ifremer.fr/doc/00000/7377/
624 Christensen, V., Pauly, D., 1992. ECOPATH II — a software for balancing steady-state ecosystem models
625 and calculating network characteristics. Ecol. Model. 61, 169–185. doi:10.1016/0304-
626 3800(92)90016-8
627 Coppin F., Travers-Trolet M. 1989. CGFS: CHANNEL GROUND FISH SURVEY, doi:10.18142/11
628 Costalago, D., Navarro, J., Álvarez-Calleja, I., Palomera, I., 2012. Ontogenetic and seasonal changes in the
629 feeding habits and trophic levels of two small pelagic fish species. Mar. Ecol. Prog. Ser. 460, 169–
630 181. doi:10.3354/meps09751
631 Cresson, P., Ruitton, S., Ourgaud, M., Harmelin-Vivien, M., 2014. Contrasting perception of fish trophic
632 level from stomach content and stable isotope analyses: A Mediterranean artificial reef
633 experience. J. Exp. Mar. Biol. Ecol. 452, 54–62. doi:10.1016/j.jembe.2013.11.014
634 Cresson, P., Travers-Trolet, M., Rouquette, M., Timmerman, C.-A., Giraldo, C., Lefebvre, S., Ernande, B.,
635 2017. Underestimation of chemical contamination in marine fish muscle tissue can be reduced
636 by considering variable wet:dry weight ratios. Mar. Pollut. Bull. 123, 279–285.
637 doi:10.1016/j.marpolbul.2017.08.046

638 Cresson, P., Travers-Trolet, M., Rouquette, M., Denamiel, M., Auber, A., 2018. Individual isotopic ratio
639 and trophic levels of fish species in the Eastern English Channel. SEANOE. doi:10.17882/55585
640 Denis, J., Vallet, C., Courcot, L., Lefebvre, V., Caboche, J., Antajan, E., Marchal, P., Loots, C., 2016. Feeding
641 strategy of Downs herring larvae (*Clupea harengu*s L.) in the English Channel and North Sea. J.
642 Sea Res. 115, 33–46. doi:10.1016/j.seares.2016.07.003
643 Dinmore, T., Jennings, S., 2004. Predicting abundance-body mass relationships in benthic infaunal
644 communities. Mar Ecol Progr Ser 276, 289–292.
645 Enever, R., Revill, A., Grant, A., 2007. Discarding in the English Channel, Western approaches, Celtic and
646 Irish seas (ICES subarea VII). Fish. Res. 86, 143–152. doi:10.1016/j.fishres.2007.05.013
647 France, R., Chandler, M., Peters, R., 1998. Mapping trophic continua of benthic foodwebs: body size-δ^{15}N
648 relationships. Mar. Ecol. Prog. Ser. 174, 301–306. doi:10.3354/meps174301
649 Fu, C., Shin, Y.-J., Perry, R.I., King, J., Liu, H., 2012. Exploring climate and fishing impacts in an ecosystem
650 model of the Strait of Georgia, British Columbia. Glob. Prog. Ecosyst.-Based Fish. Manag. Alsk.
651 Sea Grant Univ. Alsk. Fairbanks Fairbanks 65–85.
652 Fulton, E.A., Link, J.S., Kaplan, I.C., Savina-Rolland, M., Johnson, P., Ainsworth, C., Horne, P., Gorton, R.,
653 Gamble, R.J., Smith, A.D.M., Smith, D.C., 2011. Lessons in modelling and management of marine
654 ecosystems: the Atlantis experience. Fish Fish. 12, 171–188. doi:10.1111/j.1467-
655 2979.2011.00412.x
656 Giraldo, C., Ernande, B., Cresson, P., Kopp, D., Cachera, M., Travers-Trolet, M., Lefebvre, S., 2017. Depth
657 gradient in the resource use of a fish community from a semi-enclosed sea. Limnol. Oceanogr.
658 62, 2213–2226. doi:10.1002/lno.10561
659 Girardin, R., 2015. Ecosystem and fishers' behaviour modelling : two crucial and interacting approaches
660 to support ecosystem based fisheries management in the eastern English Channel. Lille 1.

Girardin, R., Fulton, E.A., Lehuta, S., Rolland, M., Thébaud, O., Travers-Trolet, M., Vermard, Y., Marchal, P., 2018. Identification of the main processes underlying ecosystem functioning in the Eastern English Channel, with a focus on flatfish species, as revealed through the application of the Atlantis end-to-end model. Estuar. Coast. Shelf Sci. doi:10.1016/j.ecss.2016.10.016

Grimm, V., Revilla, E., Berger, U., Jeltsch, F., Mooij, W.M., Railsback, S.F., Thulke, H.-H., Weiner, J., Wiegand, T., DeAngelis, D.L., 2005. Pattern-Oriented Modeling of Agent-Based Complex Systems: Lessons from Ecology. Science 310, 987–991. doi:10.1126/science.1116681

Grimm, V., Berger, U., DeAngelis, D.L., Polhill, J.G., Giske, J. and Railsback, S.F., 2010. The ODD protocol: a review and first update. Ecological modelling, 221(23), pp.2760-2768.

Grimm, V., Railsback, S.F., 2013. Individual-based Modeling and Ecology. Princeton University Press.

Grüss, A., Schirripa, M.J., Chagaris, D., Drexler, M., Simons, J., Verley, P., Shin, Y.-J., Karnauskas, M., Oliveros-Ramos, R., Ainsworth, C.H., 2015. Evaluation of the trophic structure of the West Florida Shelf in the 2000s using the ecosystem model OSMOSE. J. Mar. Syst. 144, 30–47.

Halouani, G., Ben Rais Lasram, F., Shin, Y.-J., Velez, L., Verley, P., Hattab, T., Oliveros-Ramos, R., Diaz, F., Ménard, F., Baklouti, M., Guyennon, A., Romdhane, M.S., Le Loc'h, F., 2016. Modelling food web structure using an end-to-end approach in the coastal ecosystem of the Gulf of Gabes (Tunisia). Ecol. Model. 339, 45–57. doi:10.1016/j.ecolmodel.2016.08.008

Heymans, J.J., Coll, M., Libralato, S., Morissette, L., Christensen, V., 2014. Global Patterns in Ecological Indicators of Marine Food Webs: A Modelling Approach. PLOS ONE 9, e95845. doi:10.1371/journal.pone.0095845

Hussey, N.E., MacNeil, M.A., McMeans, B.C., Olin, J.A., Dudley, S.F.J., Cliff, G., Wintner, S.P., Fennessy, S.T., Fisk, A.T., 2014. Rescaling the trophic structure of marine food webs. Ecol. Lett. 17, 239–250. doi:10.1111/ele.12226

ICES, 2011a. Catches in FAO area 27 by country, species, area and year. Source: Eurostat/ICES database on catch statistics - ICES 2011, Copenhagen. Format: Archived dataset in .xls and .csv format. Version 30-11-2011

ICES, 2011b. Report of the Working Group on the Assessment of Demersal Stocks in the North Sea and Skagerrak (WGNSSK) (No. ICES CM 2011/ACOM:13).

ICES, 2012. Report of the Working Group on Widely Distributed Stocks (WGWIDE) (21 - 27 August 2012 No. ICES CM 2012/ACOM:1 5). Lowestoft, United Kingdom.

Ings, T.C., Montoya, J.M., Bascompte, J., Blüthgen, N., Brown, L., Dormann, C.F., Edwards, F., Figueroa, D., Jacob, U., Jones, J.I., Lauridsen, R.B., Ledger, M.E., Lewis, H.M., Olesen, J.M., van Veen, F.J.F., Warren, P.H., Woodward, G., 2009. Review: Ecological Networks: Beyond Food Webs. J Anim. Ecol. 78, 253–269.

Jennings, S., Pinnegar, J.K., Polunin, N.V.C., Boon, T.W., 2001. Weak cross-species relationships between body size and trophic level belie powerful size-based trophic structuring in fish communities. J. Anim. Ecol. 70, 934–944. doi:10.1046/j.0021-8790.2001.00552.x

Jennings, S., Greenstreet, S., Hill, L., Piet, G., Pinnegar, J., Warr, K.J., 2002a. Long-term trends in the trophic structure of the North Sea fish community: evidence from stable-isotope analysis, size-spectra and community metrics. Mar. Biol. 141, 1085–1097. doi:10.1007/s00227-002-0905-7

Jennings, S., Pinnegar, J.K., Polunin, N.V.C., Warr, K.J., 2002b. Linking size-based and trophic analyses of benthic community structure. Mar. Ecol. Prog. Ser. 226, 77–85. doi:10.3354/meps226077

Jennings, S., Cogan, S.M., 2015. Nitrogen and carbon stable isotope variation in northeast Atlantic fishes and squids. Ecology 96, 2568–2568. doi:10.1890/15-0299.1

Jennings, S., van der Molen, J., 2015. Trophic levels of marine consumers from nitrogen stable isotope analysis: estimation and uncertainty. ICES J. Mar. Sci. 72, 2289–2300. doi:10.1093/icesjms/fsv120

Kopp, D., Lefebvre, S., Cachera, M., Villanueva, M.C., Ernande, B., 2015. Reorganization of a marine trophic network along an inshore–offshore gradient due to stronger pelagic–benthic coupling in coastal areas. Prog. Oceanogr. 130, 157–171. doi:10.1016/j.pocean.2014.11.001

Kopp, D., Lefebvre, S., Villanueva, C.-M., Ernande, B., 2011. Does the positive body-size-trophic level relationship hold at the species level? Presented at the Colloque « Vulnérabilité des écosystèmes côtiers au changement global et aux évènements extrêmes », 18-21 October 2011, Biarritz. https://archimer.ifremer.fr/doc/00161/27213/

Layman, C.A., Winemiller, K.O., Arrington, D.A., Jepsen, D.B., 2005. Body Size and Trophic Position in a Diverse Tropical Food Web. Ecology 86, 2530–2535. doi:10.1890/04-1098

Le Goff, C., Lavaud, R., Cugier, P., Jean, F., Flye-Sainte-Marie, J., Foucher, E., Desroy, N., Fifas, S., Foveau, A., 2017. A coupled biophysical model for the distribution of the great scallop *Pecten maximus* in the English Channel. J. Mar. Syst. 167, 55–67. doi:10.1016/j.jmarsys.2016.10.013

Mackinson, S., Daskalov, G., 2007. An ecosystem model of the North Sea to support an ecosystem approach to fisheries management: description and parameterisation. Cefas Sci. Ser. Tech. Rep. 142, 196.

Magozzi, S., Yool, A., Vander Zanden, H.B., Wunder, M.B., Trueman, C.N., 2017. Using ocean models to predict spatial and temporal variation in marine carbon isotopes. Ecosphere 8, e01763–n/a. doi:10.1002/ecs2.1763

Mahé, K., Bellamy, E., Delpech, J.P., Lazard, C., Salaun, M., Vérin, Y., Coppin, F., Travers-Trolet, M., 2018. Evidence of a relationship between weight and total length of marine fish in the North-eastern Atlantic Ocean: physiological, spatial and temporal variations. Journal of the Marine Biological Association of the United Kingdom 98, 617–625. doi:10.1017/S0025315416001752

Marzloff, M., Shin, Y.-J., Tam, J., Travers, M., Bertrand, A., 2009. Trophic structure of the Peruvian marine ecosystem in 2000–2006: Insights on the effects of management scenarios for the hake fishery

using the IBM trophic model Osmose. J. Mar. Syst. 75, 290–304. doi:10.1016/j.jmarsys.2008.10.009

Mialet B., Banaru D., Baudrier J., Bustamante P., Chekri R., Cresson P., Harmelin M., Le Loc'h F., Mauffret A., Marchand P., Petit L., Prieur S., Saibi-Yedjer L., Serre S., Spitz J., Timmerman C.-A., Vouriot P., Wessel N. 2017. Bilan des essais et optimisation du suivi mutualisé « réseaux trophiques et contaminants » sur les campagnes halieutiques DCF 2014- 2015. Rapport pour le projet DCSMM. https://archimer.ifremer.fr/doc/00373/48447/

Oliveros-Ramos, R., Shin Y-J. 2016. calibrar: an R package for the calibration of complex ecological models. arXiv:1603.03141

Oliveros-Ramos, R., Verley, P., Echevin, V., Shin, Y.-J., 2017. A sequential approach to calibrate ecosystem models with multiple time series data. Prog. Oceanogr. 151, 227–244. doi:10.1016/j.pocean.2017.01.002

Pauly, D., Christensen, V., Walters, C., 2000. Ecopath, Ecosim, and Ecospace as tools for evaluating ecosystem impact of fisheries. ICES J. Mar. Sci. 57, 697–706. doi:10.1006/jmsc.2000.0726

Pauly, D., Zeller, D., 2016. Catch reconstructions reveal that global marine fisheries catches are higher than reported and declining. Nat. Commun. 7, 10244. doi:10.1038/ncomms10244

Pethybridge, H.R., Choy, C.A., Polovina, J.J., Fulton, E.A., 2018. Improving Marine Ecosystem Models with Biochemical Tracers. Annu. Rev. Mar. Sci. 10, 199–228. doi:10.1146/annurev-marine-121916-063256

Pinnegar, J.K. 2014. DAPSTOM - An Integrated Database & Portal for Fish Stomach Records. Version 4.7. Centre for Environment, Fisheries & Aquaculture Science, Lowestoft, UK. February 2014, 39pp.

Quinn, T.J., Deriso, R.B., 1999. Quantitative Fish Dynamics. Oxford University Press.

Ramos, R., González-Solís, J., 2012. Trace me if you can: the use of intrinsic biogeochemical markers in marine top predators. Front. Ecol. Environ. 10, 258–266. doi:10.1890/110140

Robinson, L.A., Greenstreet, S.P.R., Reiss, H., Callaway, R., Craeymeersch, J., de Boois, I., Degraer, S., Ehrich, S., Fraser, H.M., Goffin, A., Kröncke, I., Jorgenson, L.L., Robertson, M.R., Lancaster, J., 2010. Length–weight relationships of 216 North Sea benthic invertebrates and fish. Journal of the Marine Biological Association of the United Kingdom 90, 95–104. doi:10.1017/S0025315409991408

Romanuk, T.N., Hayward, A., Hutchings, J.A., 2011. Trophic level scales positively with body size in fishes. Glob. Ecol. Biogeogr. 20, 231–240. doi:10.1111/j.1466-8238.2010.00579.x

Schafer, L. N., Platell, M. E., Valesini, F. J., & Potter, I. C. (2002). Comparisons between the influence of habitat type, season and body size on the dietary compositions of fish species in nearshore marine waters. Journal of Experimental Marine Biology and Ecology, 278(1), 67-92. doi:10.1016/S0022-0981(02)00337-4

Scheffer, M., Baveco, J. M., DeAngelis, D. L., Rose, K. A., & van Nes, E. (1995). Super-individuals a simple solution for modelling large populations on an individual basis. Ecological modelling, 80(2-3), 161-170.

Seibold, S., Cadotte, M.W., MacIvor, J.S., Thorn, S., Müller, J., 2018. The Necessity of Multitrophic Approaches in Community Ecology. Trends Ecol. Evol.33, 754–764. doi:10.1016/j.tree.2018.07.001

Shin, Y.-J., Cury, P., 2004. Using an individual-based model of fish assemblages to study the response of size spectra to changes in fishing. Can. J. Fish. Aquat. Sci. doi:10.1139/f03-154

Shin, Y.-J., Cury, P., 2001. Exploring fish community dynamics through size-dependent trophic interactions using a spatialized individual-based model. Aquat. Living Resour. 14, 65–80. doi:10.1016/S0990-7440(01)01106-8

Stehlik, L.L., Meise, C.J., 2000. Diet of winter flounder in a New Jersey estuary: Ontogenetic change and spatial variation. Estuaries 23, 381–391. doi:10.2307/1353330

779 Travers, M., Shin, Y.-J., Jennings, S., Machu, E., Huggett, J.A., Field, J.G., Cury, P.M., 2009. Two-way
780 coupling versus one-way forcing of plankton and fish models to predict ecosystem changes in the
781 Benguela. Ecol. Model., 220, 3089–3099. doi:10.1016/j.ecolmodel.2009.08.016
782 Travers-Trolet, M., Shin, Y.-J., Field, J.G., 2014. An end-to-end coupled model ROMS-N2P2Z2D2-OSMOSE
783 of the southern Benguela foodweb: parameterisation, calibration and pattern-oriented
784 validation. Afr. J. Mar. Sci. 36, 11–29. doi:10.2989/1814232X.2014.883326
785 Van Denderen, P.D., Lindegren, M., MacKenzie, B.R., Watson, R.A., Andersen, K.H., 2018. Global patterns
786 in marine predatory fish. Nature Ecol. Evol 2, 65–70. doi:10.1038/s41559-017-0388-z
787 Vanhoutte-Brunier, A., Fernand, L., Ménesguen, A., Lyons, S., Gohin, F., Cugier, P., 2008. Modelling the
788 Karenia mikimotoi bloom that occurred in the western English Channel during summer 2003.
789 Ecol. Model. 210, 351–376. doi:10.1016/j.ecolmodel.2007.08.025
790 Vaz, S., Carpentier, A., Coppin, F., 2007. Eastern English Channel fish assemblages: measuring the
791 structuring effect of habitats on distinct sub-communities. ICES J. Mar. Sci. 64, 271–287.
792 doi:10.1093/icesjms/fsl031

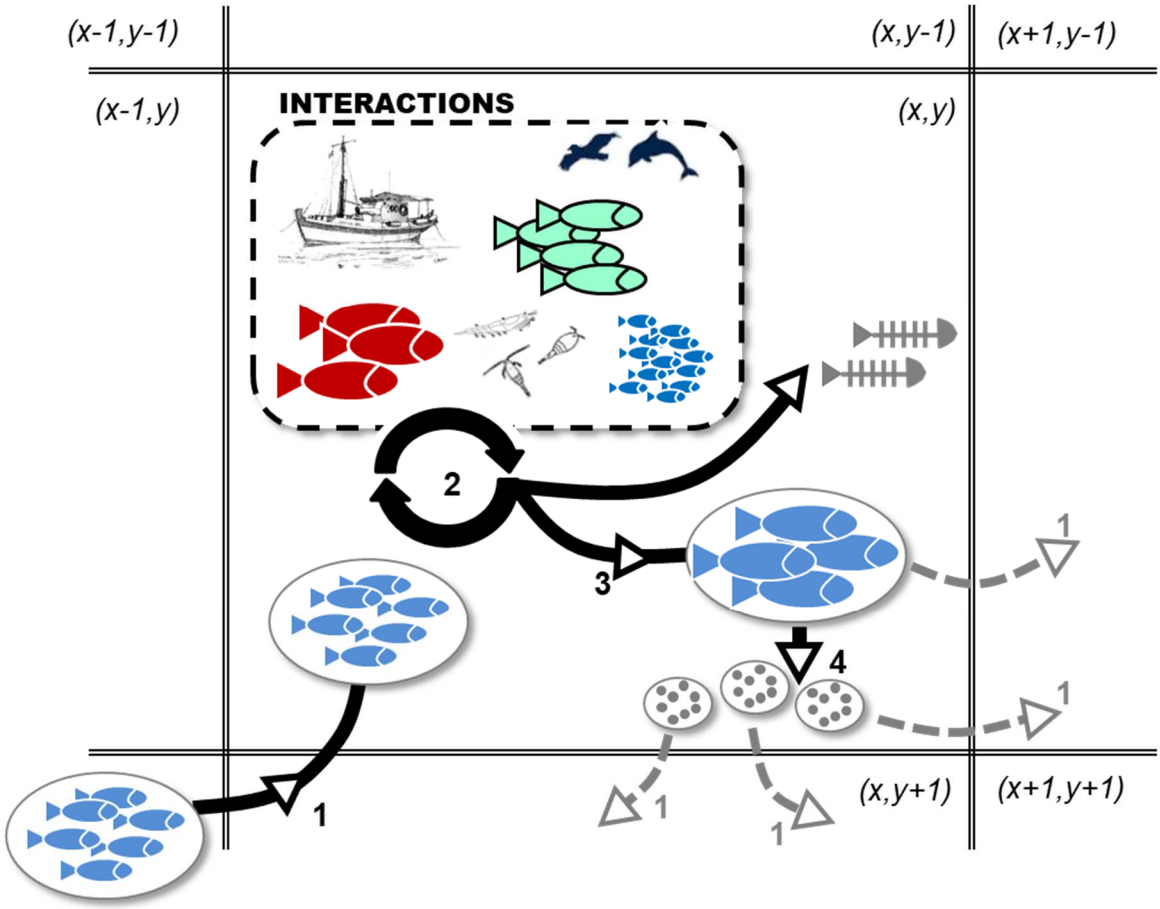

Figure 1: Processes undertaken by a superindividual during a 2-week time step : 1) Movement of individual in a 2D grid either driven by input maps or due to random walk; 2) local interactions and resulting mortalities (explicit predation mortality upon other superindividuals and upon plankton and benthos groups present in the same cell, starvation mortality, fishing mortality and mortality from other sources) looping over 10 subdivisions of the time step in order to approximate real continuous time; 3) growth proportionally to predation efficiency and 4) reproduction which creates new superindividuals of eggs for the next time step.

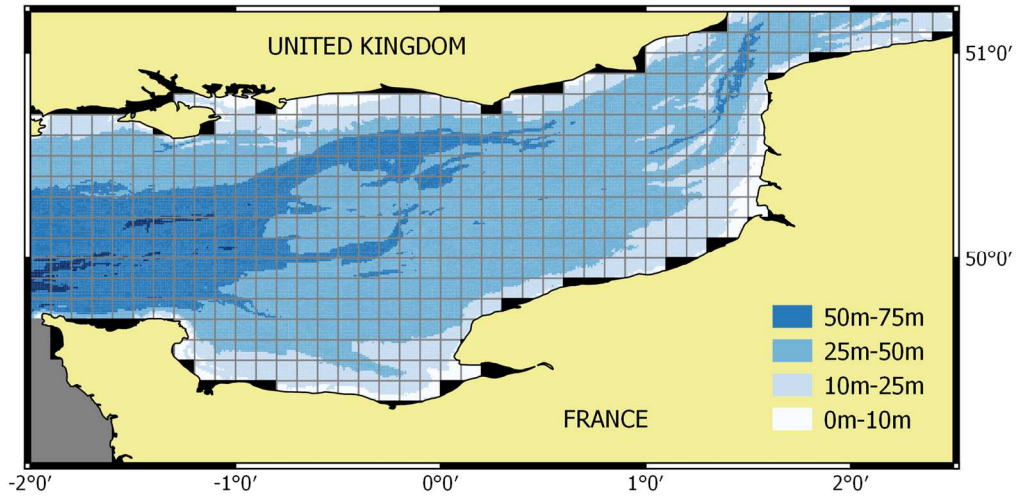

Figure 2: Grid corresponding to the modeled EEC (0.6° x 0.6° cells) with indication of depth (from GEBCO website)

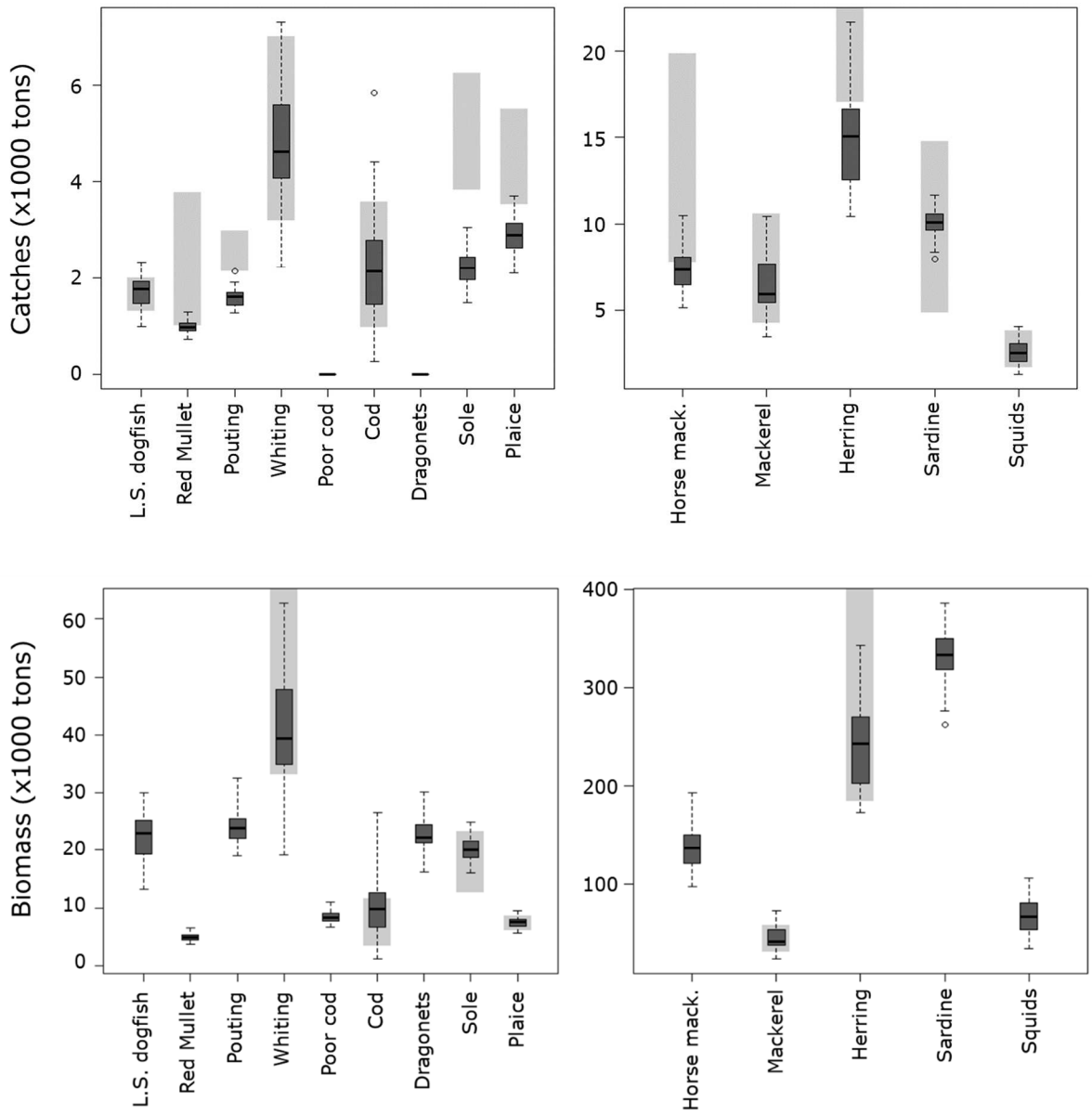

Figure 3: Distribution of the simulated catches (top) and biomass (bottom) over the 50 replicates (dark boxplots representing median and quartiles), and comparison with observations: minimal and maximum values of catches over 2000-2009 are indicated in the top panels by the grey bars. Minimum and maximum estimated biomass values are only presented for assessed species in the bottom panels.

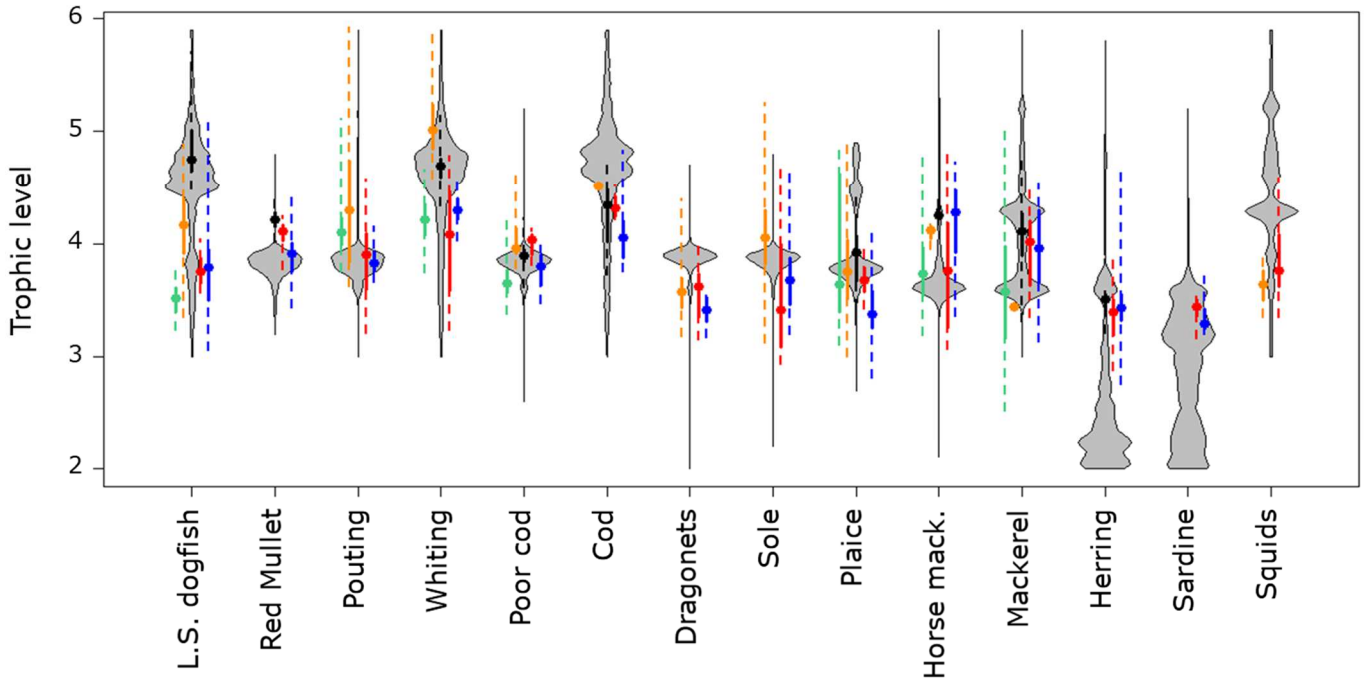

Figure 4: Modelled distribution of species biomass across TLs (trophic spectra, in grey), and comparison with published TLs for these species in the same area based on stable isotopes analysis (in green: Cresson et al. (2017), in orange: Jennings and van der Molen (2015), in black: Mialet et al. (2017), in red: Cresson et al. (2018), in blue: Kopp et al., (2015)). For SI-derived TL, the dotted line represents the range of TL measured (from minimal value to maximal value), the bold line represent values between the 1st and the 3rd quartiles and the filled dot represent the median values. Number of samples used in each study is reported in Table 4.

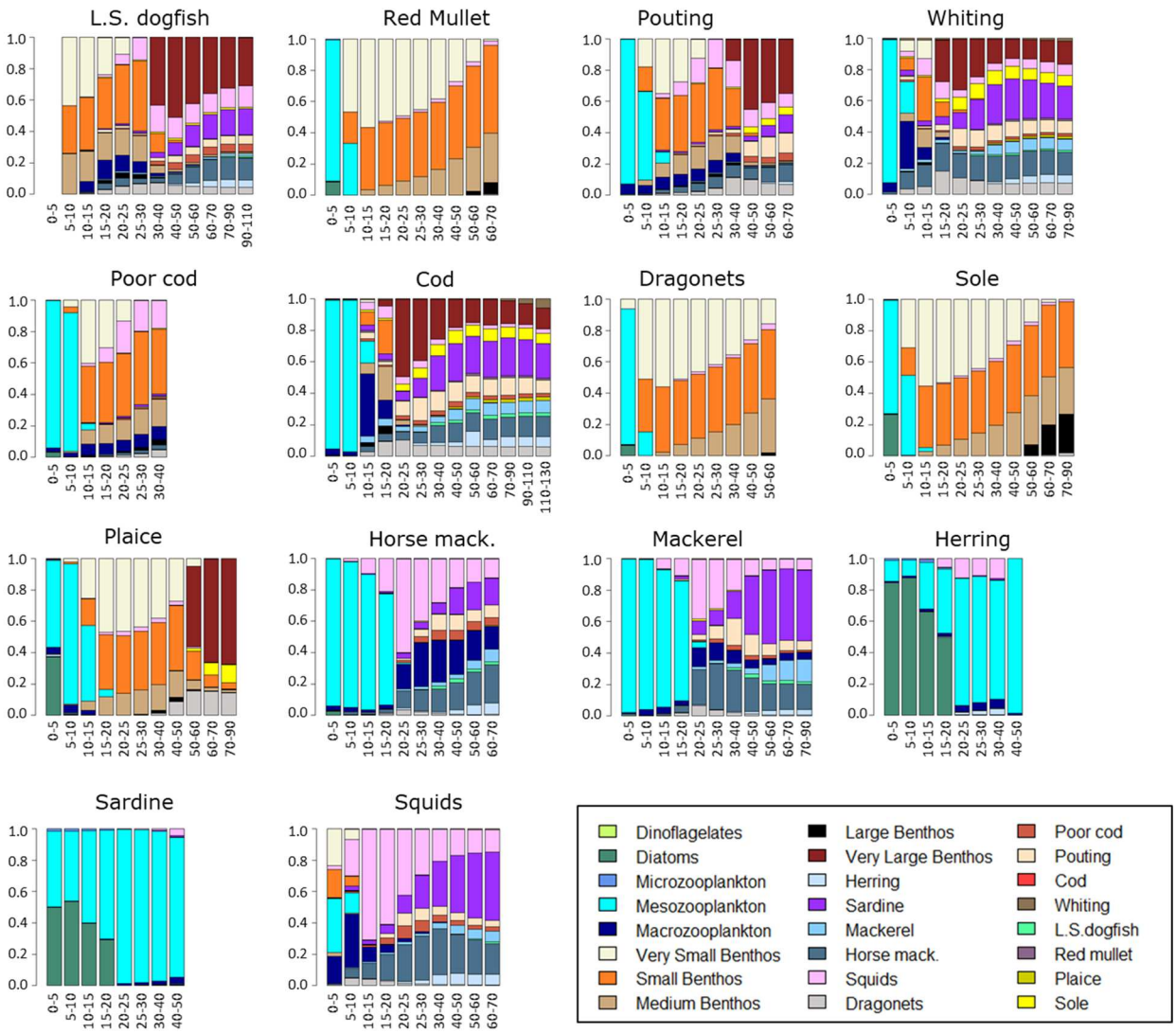

Figure 5: Emerging diet composition across size classes for the 14 modelled species over the entire area. Size classes are not regular in order to emphasize the rapid diet change of smaller individuals. Prey are grouped by species but include individuals of various length within a species group.

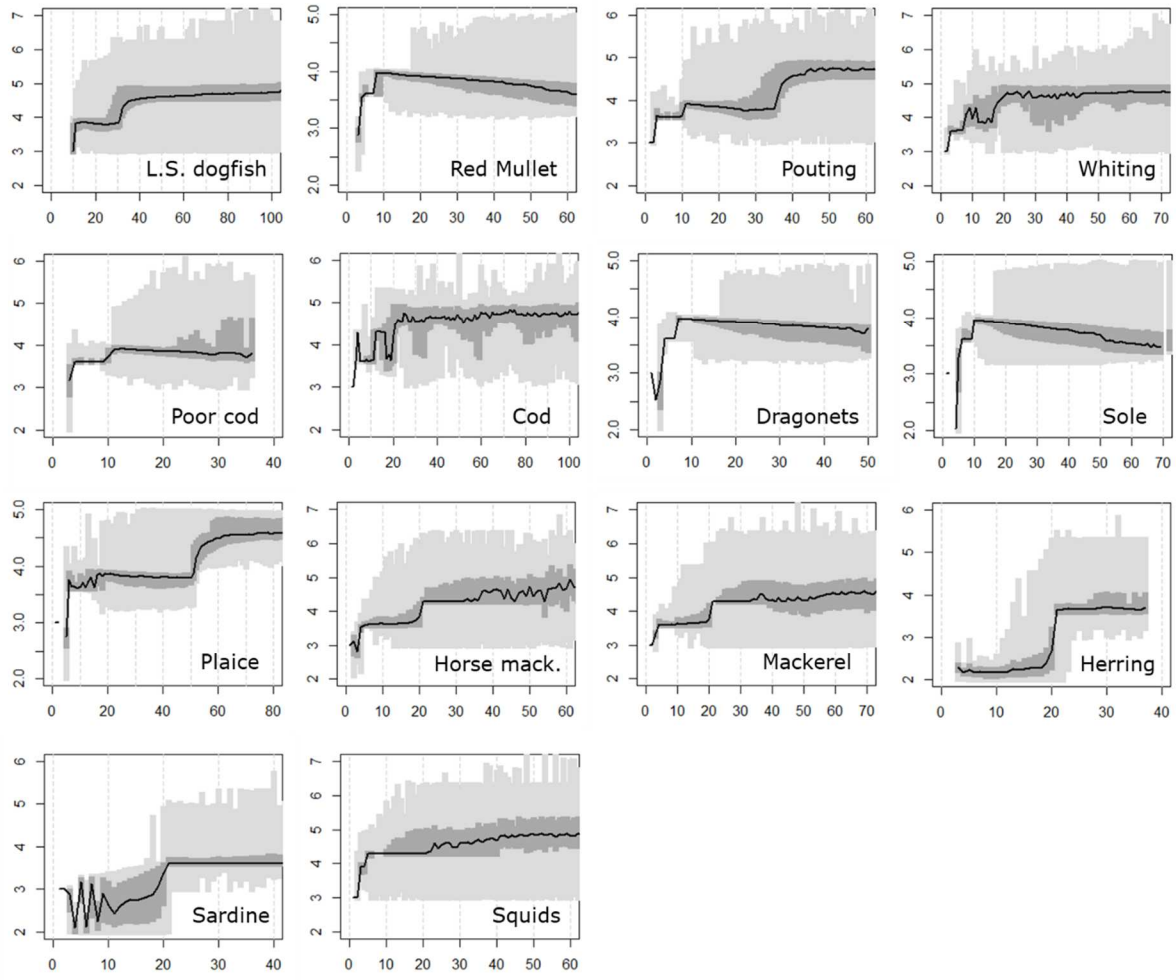

Figure 6: Modelled distribution of superindividuals' TL across 1-cm size classes for the simulated species. The light grey areas indicate minimal and maximal individual TL per centimeter, the dark grey areas indicate the 1st and 3rd quantiles of the TL distribution per centimeter and the black lines indicate the median TL per centimeter.

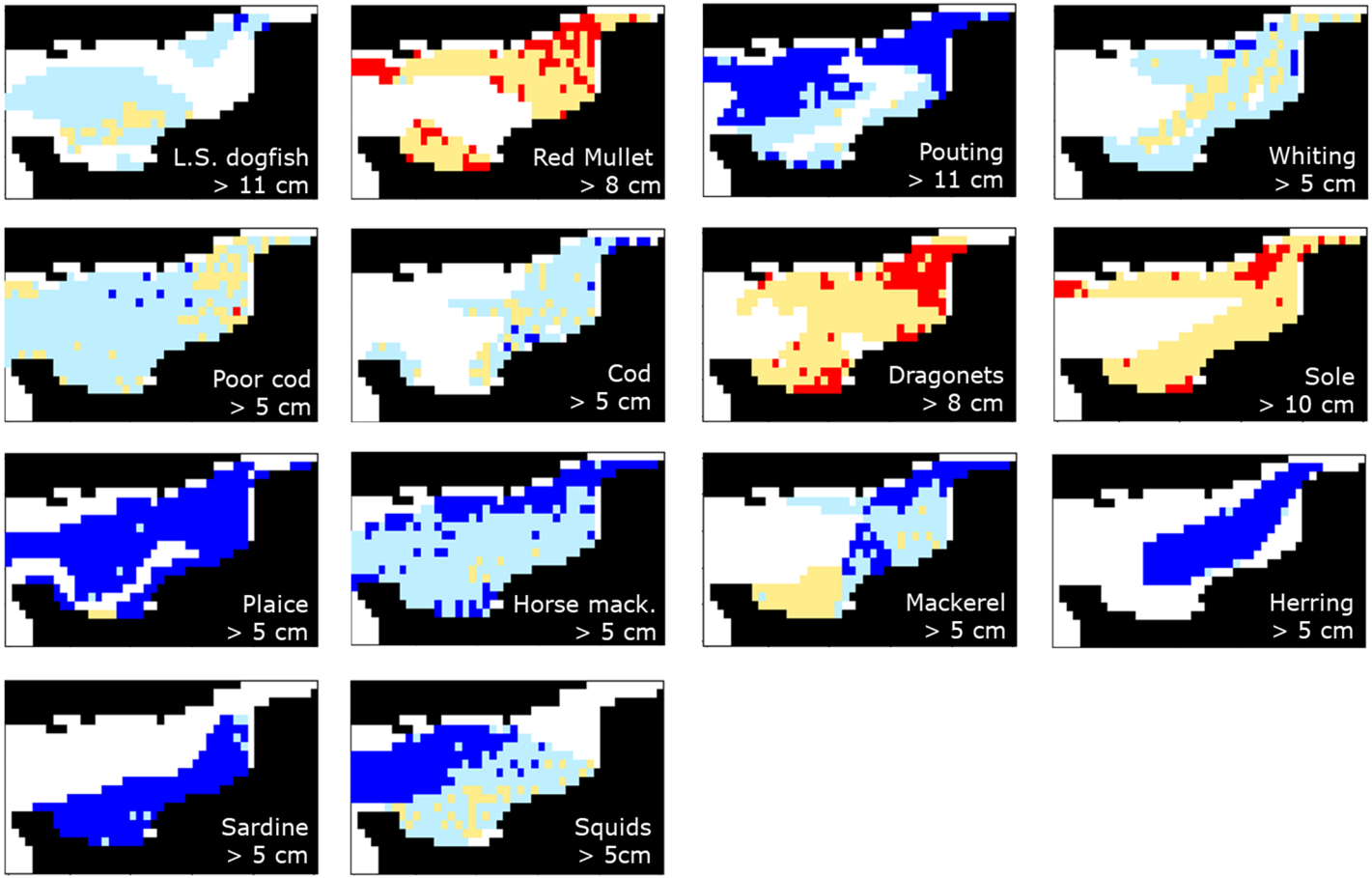

Figure 7: Spatial distribution of the direction of the TL-size relationship. In each cell with more than 10 superindividuals, a linear model has been applied between TL and size. Dark blue: positive slope with $R^2 > 0.3$; light blue: positive slope with $R^2 < 0.3$; orange: negative slope with $R^2 < 0.3$; red: negative slope with $R^2 > 0.3$.

Table 1: Input parameters of OSMOSE for the 14 fish species modelled explicitly. L_∞, K, and t_0 are the parameters of the von Bertalanffy growth model, with a linear growth before the threshold age a_{th} and a growth following the von Bertalanffy model after a_{th}; c is Fulton's condition factor and b the exponent of the L-W allometric relationship; L_{mat} is length at maturity and φ is relative fecundity; a_{max} is longevity; F is the annual fishing mortality rate and a_{rec} is age of recruitment; M_{oth} is an additional mortality rate (resulting from predation by other species of the ecosystem that are not explicitly modelled); $M_{\xi\,max}$ is the maximum starvation mortality rate, M_L is the larval mortality rate applied to the first life stage; min and max size ratios define suitable prey size for a predator, ξ_{crit} is the critical predation efficiency corresponding to maintenance requirements, max ingestion rate corresponds to the maximum amount of food edible per year relatively to the predator mass. Values reported in the table come from literature (references in Appendix 1) except from M_{oth}, F and M_L which come from calibration.

	GROWTH AND CONDITION						REPRODUCTION		SURVIVAL						PREDATION			
Species	L_∞	K	t_0	a_{th}	c	b	L_{mat}	φ	a_{max}	F	a_{rec}	M_{oth}	$M_{\xi\,max}$	M_L	Min size ratio	Max size ratio	ξ_{crit}	max ingestion rate
	cm	y^{-1}	*y*	*y*	$g.cm^{-3}$		*cm*	$eggs.g^{-1}$	*y*	y^{-1}	*y*	y^{-1}	y^{-1}	$month^{-1}$				$g.g^{-1}$
Lesser spotted dogfish	87.4	0.118	-1.09	0.5	0.00308	3.029	57	0.14	10	0.09	4	0.087	0.3	4.29	50	3	0.57	3.5
Red mullet	53.3	0.18	-1.23	1	0.00716	3.178	16.7	500	11	0.194	0.4	0	0.3	13.01	125	10	0.57	3.5
Pouting	37.6	0.46	-0.77	0.5	0.00657	3.202	23	620	4	0.106	1	0.12	0.3	6.69	50	3.5	0.57	3.5
Whiting	40.2	0.63	-0.37	1	0.00621	3.103	20	797	20	0.122	1	0.405	0.3	17.03	30	1.5	0.57	3.5
Poor cod	22.2	0.462	-0.679	0.5	0.0092	3.026	13	100	3	0	1	0.085	0.3	4.73	50	3.5	0.57	3.5
Cod	103.9	0.19	-0.1	0.5	0.00835	3.053	56	800	25	0.219	1	0	0.3	21.95	50 / 20*	2.3 / 1.8*	0.57	3.5
Dragonet	28.3	0.471	-0.443	0.5	0.0262	2.442	17.4	255	6	0	1	0.148	0.3	2.58	125	10	0.57	3.5
Sole	37.3	0.35	-1.61	0.5	0.00391	3.264	29	482	20	0.187	1.5	0	0.3	7.4	125	10	0.57	3.5
Plaice	71.7	0.23	-0.83	0.5	0.0103	3.017	27	255	15	0.44	1	0	0.3	13.52	125	5	0.57	3.5
Horse mackerel	39.2	0.18	-1.515	1	0.0054	3.114	22	1655	15	0.052	0.5	0	0.3	3.52	100	2.5	0.57	3.5
Mackerel	42	0.24	-2.07	1	0.00338	3.241	29	1070	17	0.142	0.5	0	0.3	7.94	100	2.5	0.57	3.5
Herring	29.2	0.37	-0.67	0.5	0.00503	3.1	25	458	11	0.156	1.5	0.008	0.3	1.24	1000	5	0.57	2
Sardine	24.6	0.79	-0.22	0.5	0.00594	3.077	15	2228	15	0.03	0.5	0.216	0.3	14.07	1000	5	0.57	3.5
Squids	50	2	0.5	0.7	0.25	2.27	30	50	2	0.036	0.5	0.298	0.3	7.97	20	1.5	0.57	3.5

*below and above 12cm respectively

Table 2: Parameters of the low trophic level (LTL) groups used in OSMOSE as forcing prey field. Size range of plankton groups correspond to size class used in biogeochemical models, and size class of benthic invertebrates are arbitrarily set to represent a discretized size spectrum. Trophic levels are either set arbitrarily (identified by *) or derived from SI-derived estimates from (Kopp et al., 2015) with the corresponding species indicated. Accessibility coefficients are calibrated.

	LTL groups	Size range (cm)	Trophic level	Accessibility coefficient
PELAGIC PREY	Dinoflagellates	0.0002 – 0.002	1*	$10^{-3.98}$
	Diatoms	0.002 – 0.02	1*	$10^{-2.79}$
	Micro-zooplankton	0.002 – 0.02	2*	$10^{-0.97}$
	Meso-zooplankton	0.02 – 0.2	2.6 (copepods)	$10^{-0.37}$
	Macro-zooplankton	0.2 – 2	3.8 (*Crangon crangon*)	$10^{-1.56}$
BENTHIC PREY	Very small benthos	0.02 – 0.5	3*	$10^{-1.20}$
	Small benthos	0.5 – 1	2.9 (*Nereis sp.*)	$10^{-1.30}$
	Medium benthos	1 – 5	2.2 (bivalves)	$10^{-1.87}$
	Large benthos	5 – 10	2.3 (*Psammechinus miliaris*)	$10^{-2.96}$
	Very large benthos	10 – 15	3.6 (*Maja brachydactyla*)	$10^{-0.38}$

Table 3: Accessibility coefficients between individuals depending on their vertical position, representing the proportion of prey biomass available to a predator. The vertical position of individuals depends on their stage and is indicated in the last column.

		Predator			
		Pelagic	Demersal	Benthic	
Prey	Pelagic	1	0.5	0	Red mullet, Pouting, Whiting, Dragonet, Plaice younger than 3 months Cod younger than 0.4 year Sole younger than 0.15 year Horse mackerel, Mackerel, Herring, Sardine Dinoflagellates, Diatoms, Microzooplankton, Mesozooplankton, Macrozooplankton
	Demersal	0.5	1	0	Lesser spotted dogfish older than 0.45 year, Pouting, Whiting older than 3 months Cod older than 0.4 year Squids older than 1.5 month
	Benthic	0	0.5	1	Lesser spotted dogfish younger than 0.45 year, Red mullet, Dragonet, Plaice older than 3 months Sole older than 0.15 year Squids younger than 1.5 month Very small benthos, Small benthos, Medium-size benthos, Large benthos, Very large benthos

Table 4: Size range and number of fish individuals (N) used to estimate species TL based on SI measurement in four empirical studies realized in the EEC. For Jennings and Cogan (2015), body size are estimated from body mass using allometric relationship (Robinson et al. 2010; Mahé et al. 2018). Squid length was estimated based on an unpublished relationship (ln(Length)= 2.86 + 0.44 ln(mass) calculated on individual length-mass measurement performed during CAMANOC survey in the English Channel (K. Mahé, Ifremer Halieutic Information System, pers. comm.)

	Kopp et al., 2015	Jennings and Cogan, 2015	Mialet et al. 2017	Cresson et al., 2017	Cresson et al., 2018
Lesser spotted dogfish	11-64 cm N=36	17-63.7 cm N=53	40-63 cm N = 18	42-67.9 cm N=25	50.5-65 cm N=10
Red mullet	7-32 cm N=63	N=0	20-25 cm n=5	N=0	15-19.6 cm N=10
Pouting	9-27.5 cm N=24	7.9-33.9 cm N=37	n=0	12.9-32.9 cm N=50	11.9-22.7 cm N=19
Whiting	7-41 cm N=39	12.5-32.7 cm N=28	21-38 cm N=30	14.6-35 cm N=80	6.8-36.4 cm N=16
Poor cod	10.6-21.5 cm N=12	7.2-19.3 cm N=27	9-12 cm n=9	8.4-17.5 cm N=77	9.3-15.6 cm N=10
Cod	35-73 cm N=33	36cm N=1	29-93 cm N=18	N=0	33.2-68.7 cm N=8
Dragonet	9-23 cm N=18	5.8-24.5 cm N=83	N=0	N=0	12-18.7 cm N=15
Sole	9-38 cm N=51	12.7-36.7 cm N=78	N=0	N=0	7.5-29.5 cm N=1
Plaice	9-43 cm N=37	8.5-55.3 cm N=134	20-38 cm n=40	22.5-42.6 cm N=28	13.4-25 cm N=15
Horse mackerel	8-39 cm N=54	19.6-21.4 cm N=7	10-13 cm N=7	11.4-31.5 cm N=148	4.3-20.4 cm N=23
Mackerel	18-37 cm N=39	32cm N=1	30-34 cm N=6	16.9-41 cm N=158	24.3-28.9 cm N=10
Herring	6.2-29 cm N=10	N=0	5-27 cm N=6	N=0	7-25.1 cm N=15
Sardine	7.7-29 cm N=10	N=0	N=0	N=0	9.8-20.2 cm N=10
Squids	N=0	11.5-16.8 cm N=4	N=0	N=0	9-31 cm N=17